The applicability of Raman spectroscopy in the assessment of palaeowildfire intensity

Thomas Theurer[1], David K. Muirhead[1], David Jolley[1] and Dmitri Mauquoy[1]

[1]School of Geosciences, University of Aberdeen, King's College, Aberdeen, AB24 3UE, UK

Corresponding author: Thomas Theurer (t.theurer.19@abdn.ac.uk)

Keywords: Charcoal; Pyrolysis; Microstructure; Organic carbon

Abstract

Evidence of wildfires in deep time is preserved as fossilised charcoal fragments in the rock record and inertinite macerals in coal. Historically, charcoal reflectance has been utilised to assess the formation temperature of these charcoals, and thus burning intensities of prehistoric fires. This is achieved by quantifying reflectance variability as a function of changes in charcoal microstructure with temperature. Raman spectroscopy been shown to similarly assess microstructure in carbonaceous organic matter with thermal maturation. However, there have been few applications of Raman spectroscopy to wildfire-derived charcoals, modern or prehistoric. Little consideration has also been paid to the nature and applicability of derived parameters in assessing intensity. This study presents a novel assessment of Raman spectroscopy as a method for interpreting palaeowildfire burning intensity. Spectra were obtained from experimentally pyrolysed *Calluna vulgaris* material, generated across a range of natural wildfire temperatures, and subsequent derived parameters were compared with established principles. For assessing changes in palaeowildfire intensity, this study has found the best correlations between thermal maturity and; D-band full-width at half-maximum (D-FWHM) and the D-/G-band full-width at half-maximum ratio (D-FWHM/G-FWHM). Additional parameters, commonly applied to Raman studies of charcoal, are otherwise influenced by non-linearity. The influence of precursor material on charcoal microstructure has also been derived, indicating further complexity when assessing heterogenous samples. Our results indicate that, whilst Raman spectroscopy offers extraordinary potential for understanding prehistoric and modern wildfire intensity, parameters and further analyses used require measured consideration.

1. Introduction

Recent developments in the global interaction between wildfires and climate have elevated the importance of understanding the factors that influence changing fire regimes. In order to discern the future of wildfires under anthropogenic climate change, understanding palaeowildfires associated with archaeological and geological records may prove beneficial. Whilst modern fires are primarily characterised by the influence of vegetation fuel type, weather and topography (Scott, 2000 after Pyne et al., 1996) often associated with human ignition, the resolution of geological preservation often limits such evidence for palaeowildfires. Instead, we may better categorise palaeowildfires by assessing long term

climatic, vegetational and atmospheric changes (Scott, 2000). These factors directly relate to fire intensity, representing a significant component of palaeowildfires that may be quantified via the assessment of temperature.

Palaeowildfire temperature has historically relied on reflectance analysis of pyrolysed biomass - charcoal or 'fusain' (Scott, 1989). This may be preserved in sediments, or within coals as inertinite macerals (Scott, 1989, 2000; Glasspool, 2000; Diessel, 2010; Abu Hamad et al., 2012; Jasper et al., 2013). Since the initial derivation of the relationship between reflectance and charcoal formation (pyrolysis) temperature (Jones et al., 1991) many studies have utilised charcoal reflectance to understand how wildfires have occurred and progressed through geological time (e.g. Bojesen-Koefoed et al., 1997; Scott, 2000; Edwards and Axe, 2004; Glasspool et al., 2004, 2006; Marynowski et al., 2011; Shen et al., 2011; Petersen and Lindstrom, 2012; Uhl et al., 2014; Hudspith et al., 2015; Rimmer et al., 2015; Cardoso et al., 2018; Benecio et al., 2019). The aim of applying charcoal reflectance to fossil charcoals is to understand the 'anatomy' of a fire and its vegetation, utilising three thermo-limitational subgroups of fire; smoldering (ground), surface, and crown (Scott, 1989 after Davis, 1959). However, more recent characterisations of wildfires (see Section 1.1) have recorded instances of overlap between typical crown, surface and smoldering temperatures, suggesting the requirement of palaeoecological and palynological context when assessing palaeowildfires. This is further complicated by definitive shifts in recorded reflectance values and subsequent formation temperatures in modern fires, dependent on the precursor plant material (Hudspith et al., 2014). Instead, the assessment of changes to wildfire intensity patterns may better offer an insight into the structure and nature of fuels associated with a particular wildfire regime, without need for a quantitative temperature reconstruction.

1.1 Characterising wildfire temperatures

Smoldering ground fires typically occur within the subsurface biomass and characterise much of the burning we observe in modern (Rein et al., 2008) and historic peatland fires (Mauquoy et al., 2020). In contrast, surface fires occur across the ground surface, consuming low growing plant material and litter (Scott, 1989). When a fire reaches the uppermost flammable material in the crown of a tree, it is designated a crown fire (Scott, 1989), often propagated from surface fires via 'ladder fuels' (Menning and Stephens, 2007).

Historical thresholds have characterised smoldering, surface and crown fires as <350°C, 350-600°C and >600°C respectively (Rundel, 1981; Scott and Jones, 1994; Scott, 2000; Rimmer et al., 2015). These values may now be considered outdated, given significant variability in natural temperatures identified within modern wildfire systems. Temperatures between 450°C and 700°C are now considered more representative of smoldering fires (Rein et al., 2008; Rein, 2016) whilst burning in modern eucalypt forests (Wotton et al., 2012) has reported little variability in temperatures observed between surface (~670-1100°C) and crown fuels (~680-1180°C). Maximum boreal crown fire temperatures have exceeded 1200-1300°C (Butler et al., 2004; Taylor et al., 2004) though it has been suggested flaming fires may reach 1500°C (Drysdale, 1998; Rein et al., 2008).

1.2 Raman spectroscopy and wildfires

Charcoal reflectance, reliant on changes in reflectivity as a function of microstructure to quantify temperature (Scott, 2010), is similar in process to vitrinite reflectance – a method of assessing thermal maturity in organic material. Vitrinite reflectance has been shown to correlate well with Raman spectroscopy in the assessment of organic maturation (Quirico et al., 2005; Guedes et al., 2010; Hinrichs et al., 2014; Lünsdorf, 2016; Schito et al., 2017; Wilkins et al., 2014, 2015, 2018; Henry et al., 2019a, 2019b; Muirhead et al., 2019). However, little work has utilised charcoal reflectance and Raman spectroscopy simultaneously (Ascough et al., 2010).

The application of Raman to charcoals, however, has been limited primarily to the understanding of microstructural change in wood with pyrolysis (e.g. Ishimaru et al., 2007b). The understanding of wildfire intensity and associated climatic and vegetation changes, via the application of Raman spectroscopy, has only been approached once so far. In Mauquoy et al. (2020) a succession of charcoal preserved in an 11550 BP Falkland Island peat profile was analysed using Raman spectroscopy – identifying fluctuations in wildfire intensity associated with fire-favorable moisture and vegetational changes. All other relevant Raman applications are limited to Quaternary charcoal material derived from modern soils (Ascough et al., 2010; Jorio et al., 2012; Ribeiro-Soares et al., 2012; Mastrolonardo et al., 2014; Inoue et al., 2017; de Sousa et al., 2020). Further investigation of Raman spectroscopy is required to better characterise the applicability of this methodology in the assessment of wildfire charcoals, formation temperature and intensity.

In this study, we present and examine Raman spectroscopic analysis of charcoals derived from experimentally pyrolysed plant material. Utilising these data, we introduce the first assessment of Raman parameters with respect to their ability to effectively quantify changes in charcoal formation temperature and equivalent intensity. This preliminary study ultimately demonstrates the requirement for targeted application of Raman parameters, consideration of the statistical nature of datasets, and recognition of the inherent heterogeneity of fossil charcoal samples.

2. Materials and Methods

2.1 Sample selection

Samples of *Calluna vulgaris* (L.) Hull (Ling Heather) were acquired between June and October 2019 in NE and NW Scotland, and separated into three broad groups: stems, roots and flowers. *Calluna* was selected primarily for its widespread nature across Scotland and intimate relationship with fire (Hudspith et al., 2015). Its small, shrubby habit also ensures it is easily sampled, prepared, and pyrolysed. Samples were separated by anatomical component in order to test results individually and assess the potential impacts of charcoal precursor material on resultant data.

2.2 Sample pyrolysis

In order to assess the applicability of Raman spectroscopy to characterising wildfire intensity changes, reference charcoals are required to calibrate changes in parameters with a range of appropriate formation temperatures, and thus, intensities. Achieving this requires the production of charcoals via the pyrolysis of plant material. Pyrolysis is the process by which biomass thermally decomposes in the absence of oxygen – perpetuated by the initial oxidative combustion of flammable gaseous (pyrolysate) products (Rein, 2013). This process draws oxygen away from the surface of biomass fuel, producing pyrolytic charcoals and ash (Tran and White, 1992; Belcher and Hudspith, 2016). Recent work has brought to light the nature of combustion within natural wildfire systems, and the understanding that both pyrolysis and oxidation occur as the flaming phase passes, and residual smoldering combustion continues (Rein, 2013; Belcher and Hudspith, 2016). Results have also indicated that heating continues within samples during this transition to a smoldering phase, which has

a direct impact on the applicability of charcoal reflectance as a quantitative assessment of wildfire temperature (Belcher and Hudspith, 2016; Hudspith and Belcher, 2017).

The experimental generation of charcoals by wrapping plant samples in foil has been utilised historically (Orvis et al., 2005). Other common methods have included the submersion of samples in sand (Jones et al., 1991; Orvis et al., 2005), and the implementation of a controlled inert atmosphere oven – a method that has typically been used in Raman studies (Yamauchi et al., 2000; Yamauchi and Kurimoto, 2003; Paris et al., 2005; Ishimaru et al., 2007a, 2007b). More recent experimental studies, with reference to assessing charcoal reflectance, have indicated the suitability of oxygen-depletive calorimetry in replicating the conditions of wildfires (Belcher and Hudspith, 2016; Hudspith and Belcher, 2017). Contrary to applications alongside charcoal reflectance, the impact of pyrolysis methodology on Raman spectroscopic data has not been assessed in any capacity. Therefore, the application of foil-pyrolysis within this study allows for a preliminary analysis of changes in charcoal microstructure with increasing heat treatment. This is with the intention of future exploration into the impact of pyrolysis methodology on data derived from Raman spectroscopy.

Prior to charring, samples of *Calluna* were dried for 48 hours in a *Gallenkampf* 'Hotbox' oven at 70°C. This is to ensure the complete removal of free moisture, a factor that has been shown to directly influence charcoal reflectance values in charring experiments (Belcher and Hudspith, 2016). Each sample was then separated by anatomical component into the three categories (stem, root, flower). Following preparation, samples were placed into a *Carbolite* ELF 11/148 temperature-controlled laboratory furnace and heated at a rate of 5°C/min until experimental temperatures of 250, 400, 600 and 800°C – were reached. These are consistent with a range of fire temperatures observed in modern wildfire systems (Scott, 2000), including the temperature at which the earliest point of charcoalification is observed (Jones et al., 1991). Samples dwelled at the desired temperature for 90 minutes, and following pyrolysis were allowed to cool gradually to room temperature before collection. For temperatures below 800°C, samples were wrapped individually in aluminum foil, whilst samples tested at 800°C were wrapped similarly in copper foil, due to the respective melting points of aluminum (~660°C) and copper (1080°C). The duration of charring was limited to 90 minutes, given observations in reflectance stability after 60 minutes in charcoal reflectance studies (Scott and Glasspool 2007; McParland et al., 2009). This also indicates that the change in foil metal at 800°C, and subsequent differences in metal

thermal conductivity, should have little impact in the resultant degree of charcoalification. This is supported by an additional 30 minutes at the desired temperature; ensuring samples reached the correct charring temperature prior to dwelling (McParland et al., 2007) and displayed charcoalification at the lowest temperature (Jones et al., 1991).

2.3 Raman spectroscopy

Raman spectroscopy, when applied to organic carbon, relies on the quantification of the relationship between two first order spectral bands – D (disordered) and G (graphitic) (Tuinstra and Koenig, 1970). These bands ultimately reflect the changes to structural ordering, via the growth of ordered crystallite units, within carbonaceous material (Tuinstra and Koenig, 1970). Previous research has indicated the relationship between several parameters and the formation temperature of charcoal, including both natural (300-1000°C) and industrial (>1200°C) pyrolysis (Yamauchi et al., 2000; Yamauchi and Kurimoto, 2003; Paris et al., 2005; Ishimaru et al., 2007a; 2007b; Zaida et al., 2007). Whilst Raman spectroscopy has been utilised in studies regarding all components of the structural ordering process in carbon – from disordered organic carbon to homogenous graphite – the nature of charcoal limits Raman assessment wholly to amorphous maturation processes.

Charcoal samples were analysed using a *Renishaw* inVia Reflex Raman spectrometer at the University of Aberdeen, utilising an Ar+ green laser (514.5 nm). This was focused using a Leica DMLM reflected light microscope through a ×50 objective lens. A laser spot size of ~1-2 µm was achieved, employing 10% laser power. Prior to sample analysis, the laser was calibrated against a Renishaw podule-housed silicon sample, followed by manual crosshair alignment and slit-alignment where appropriate. Spectra were recorded using a coupled device detector (CCD). Spectral acquisition was centered at 1400 cm^{-1} and collected between 1100 and 1700 cm^{-1}, with a resolution of 3 cm^{-1}. Three accumulations were recorded per spectra, over a period of 15 seconds in total. Deconvolution was performed using the *Renishaw* WiRE 3.4 Curve-fit Software, followed by smoothing and baseline extraction via cubic spline interpolation. This process was implemented at least three times for each spectral acquisition, ensuring any background interference was removed, and data remained reproducible. This methodology is consistent with established processes analysing carbonaceous organic matter (Muirhead et al., 2012, 2016, 2019; Henry et al., 2018) including, specifically, the study of charcoal (Paris et al., 2005; Ishimaru et al., 2007a, 2007b;

Zaida et al., 2007). The use of reduced laser intensity (10%) resulted in a laser power of approximately 3 mW. Whilst laser power exceeding 1 mW has been suggested to cause sample combustion and an erroneous G-band shift (Henry et al., 2018) no discernible damage to the samples was noted in this instance. Up to 50 Raman measurements were taken for each sample, comprising 10 randomly selected positions across 5 individual pieces of charcoal where appropriate. Sampling was limited by visible and distinguishable charcoalification, identifiable within a sample by light reflectivity in microscopic assessment.

The data produced following deconvolution were processed into the following Raman parameters; full-width at half-maximum of the D-band (D-FWHM) and G-band (G-FWHM), D- and G-band area ratio (AD/AG), D- and G-band height ratio (ID/IG), D- and G-band peak separation (G-D) and finally, D- and G-band full-width at half-maximum ratio (D-FWHM/G-FWHM). The nature of these parameters with respect to the Raman spectral response is displayed in Figure 1. In order to reduce confusion between parameter nomenclature, the given abbreviation in Henry et al. (2019b) for ID/IG (R1) and G-D (RBS) will be implemented throughout this paper.

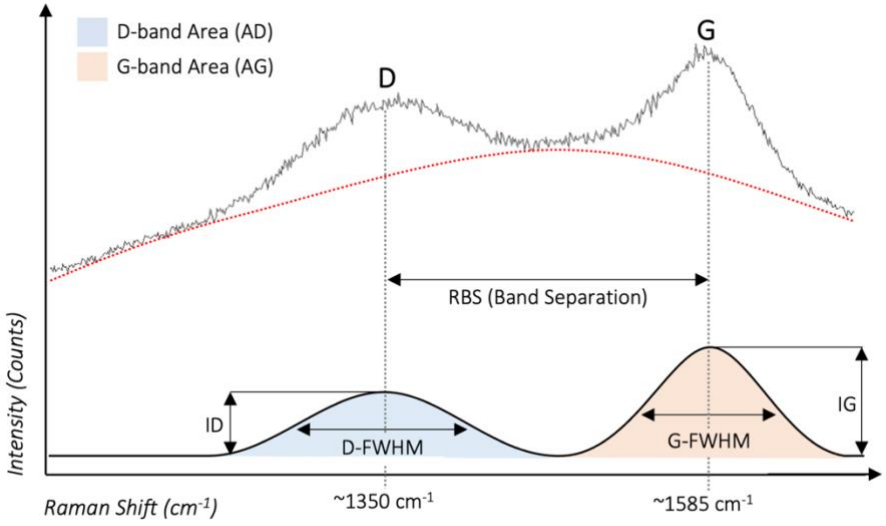

Figure 1. Schematic diagram indicating the relevant parameters and their relationship to raw (grey) and deconvolved (black) Raman spectra, following the application of a cubic spine interpolative baseline (red).

3. Results

3.1 Statistical distribution

Following distribution assessment of the Raman data in this study it is evident that, whilst there are several instances of near-normal distribution, this may change with respect to the sample and formation temperature (Figure 2). The greatest variance from normal distribution may be observed in data associated with 250°C formation temperature. Applying Shapiro-Wilk's test of normality to individual parameter-temperature datasets, assuming a null hypothesis of normal distribution, indicates only three instances where the data are normally distributed (Table 1). For all other datasets, the null hypothesis may be reliably rejected, and non-normal distribution assumed. Variation in distribution may also be observed in boxplots (Figure 3) where it is clear that 250°C charcoals display multiple outliers, typically associated with higher parameter values. The impact of this shift in distribution is indicated by the relationship between mean and median values displayed on the boxplots. At 250°C, mean values tend to be shifted toward higher parameter values as a result of the outlying data.

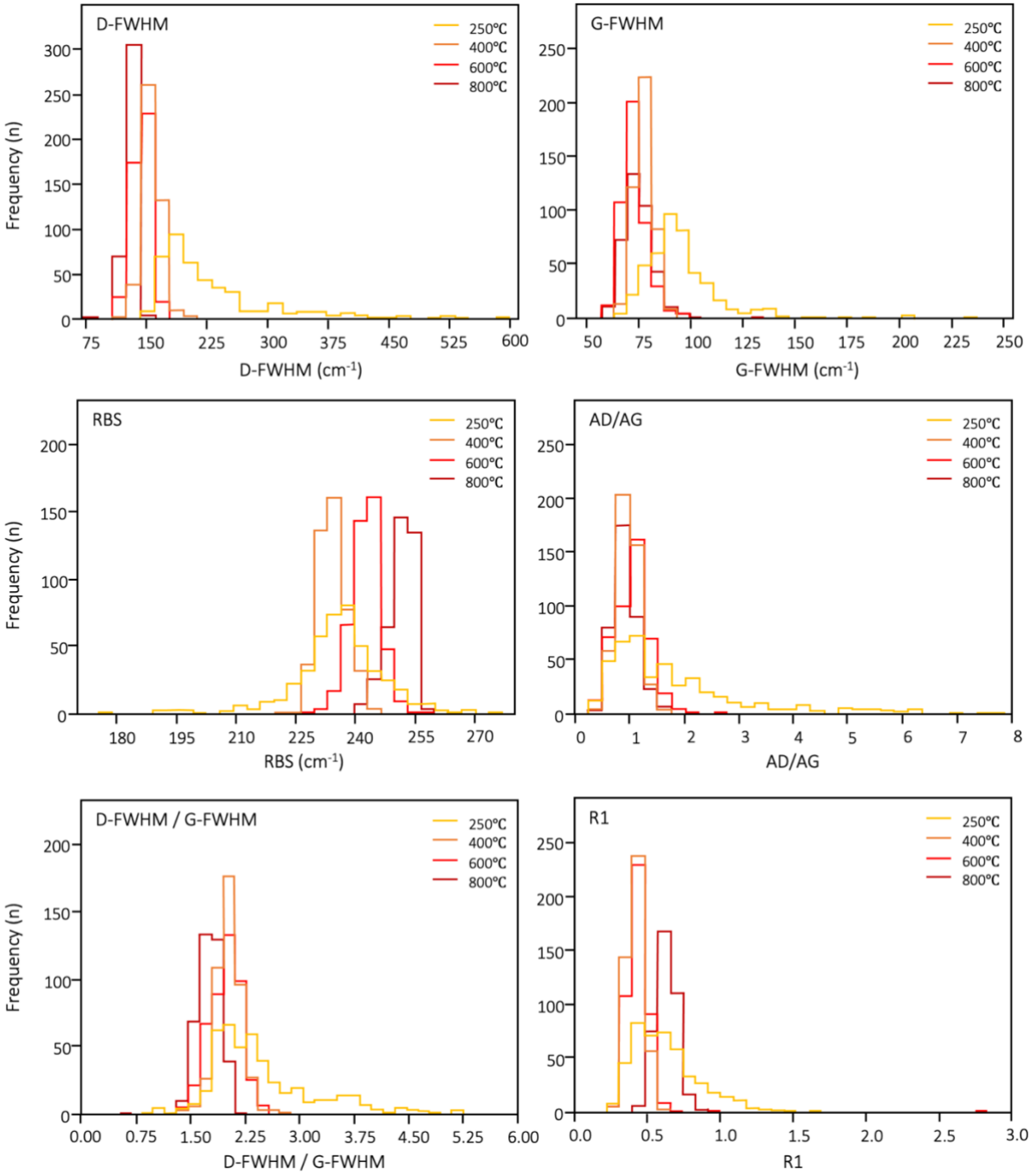

Figure 2. Stacked histograms displaying the relative distributions of data sets for each temperature across the different contributory Raman parameters.

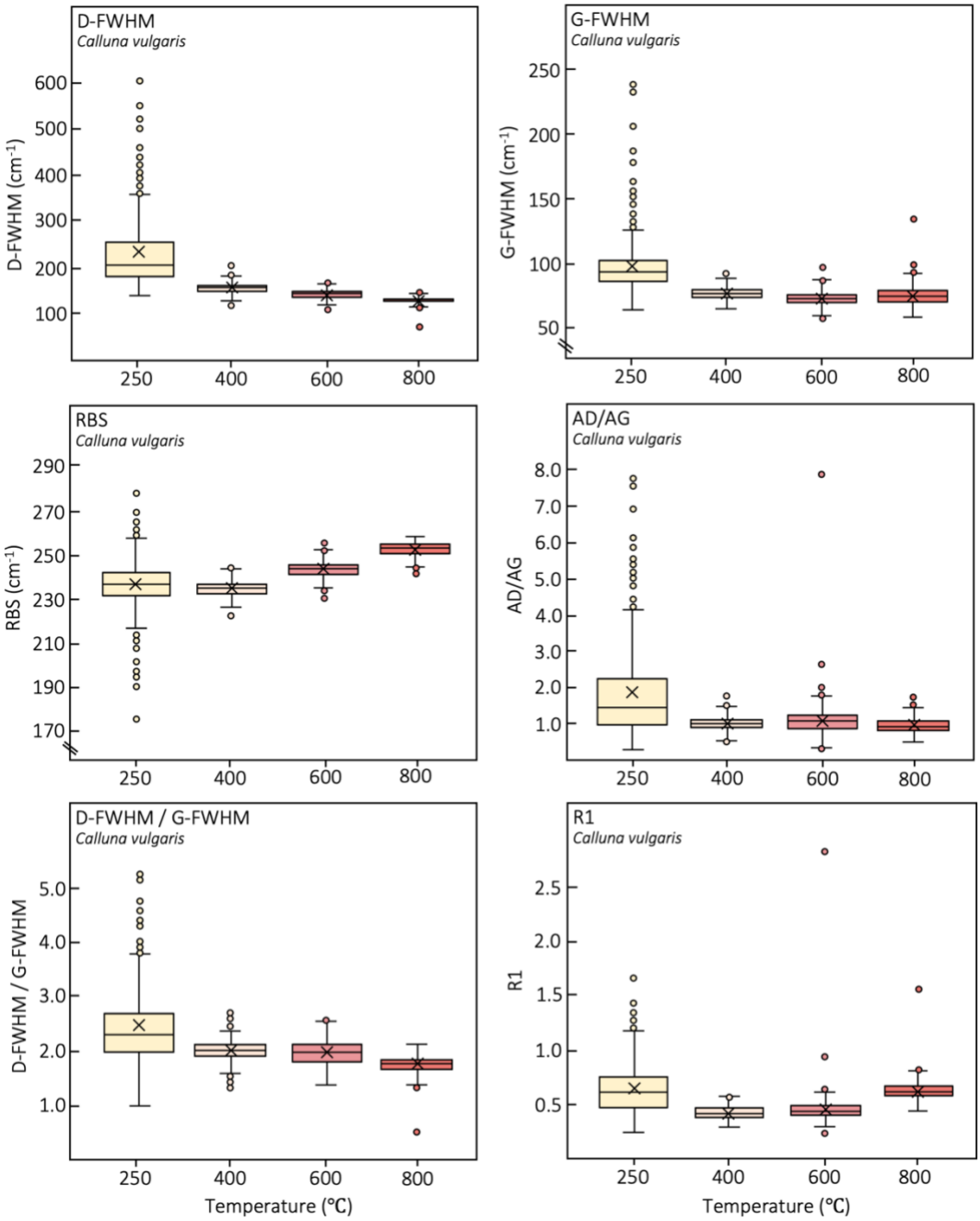

Figure 3. Box and whisker plots showing the relative distribution of data across the four tested temperatures, for each parameter. Outliers are indicated by filled circles outwith the minimum and maximum value 'whiskers', whilst mean values are denominated by a cross. Median values correspond to the central line within the interquartile range 'box'.

Parameter	°C	Shapiro-Wilk's Test of Normality		
		N	*W*	*p*(normal)
D-FWHM	250	450	0.802	<.001
	400	450	0.964	<.001
	600	450	0.982	<.001
	800	384	0.899	<.001
G-FWHM	250	450	0.770	<.001
	400	450	0.994	Not Significant
	600	450	0.961	<.001
	800	384	0.913	<.001
R1	250	450	0.935	<.001
	400	450	0.995	Not Significant
	600	450	0.405	<.001
	800	384	0.829	<.001
AD/AG	250	450	0.820	<.001
	400	450	0.991	<.01
	600	450	0.617	<.001
	800	384	0.976	<.001
RBS	250	450	0.938	<.001
	400	450	0.995	Not Significant
	600	450	0.984	<.001
	800	384	0.936	<.001
D-FWHM / G-FWHM	250	450	0.901	<.001
	400	450	0.981	<.001
	600	450	0.990	<.01
	800	384	0.939	<.001

Table 1. Results of Shapiro-Wilk's statistical assessment of normality, with respect to tested formation temperature across each Raman parameter. *N* indicates number of tested datasets, whilst values of $W<1$ represent data non-conformable to the null hypothesis. Assessment of normality is derived from *p*(normal) values, in accordance with alpha (a) level 0.05 (95% confidence). Given *p*(normal) values below a 0.05, the null may be reliably rejected, and non-normality assumed.

3.2 Raman-temperature interactions

Primary visual assessment of the typical spectra produced at each temperature indicate changes that are reflected in later analysis of parameters. In Figure 4, a narrowing of the G-band, by way of subtle width reduction and increased intensity, may be observed. This occurs simultaneously with D-band intensification and width reduction. The width between band peaks (RBS) also increases, suggesting a leftward shift of the D-band to lower

wavelengths, and a congruent shift in the G-band to higher wavenumbers. These observations are similarly reflected in data obtained following deconvolution.

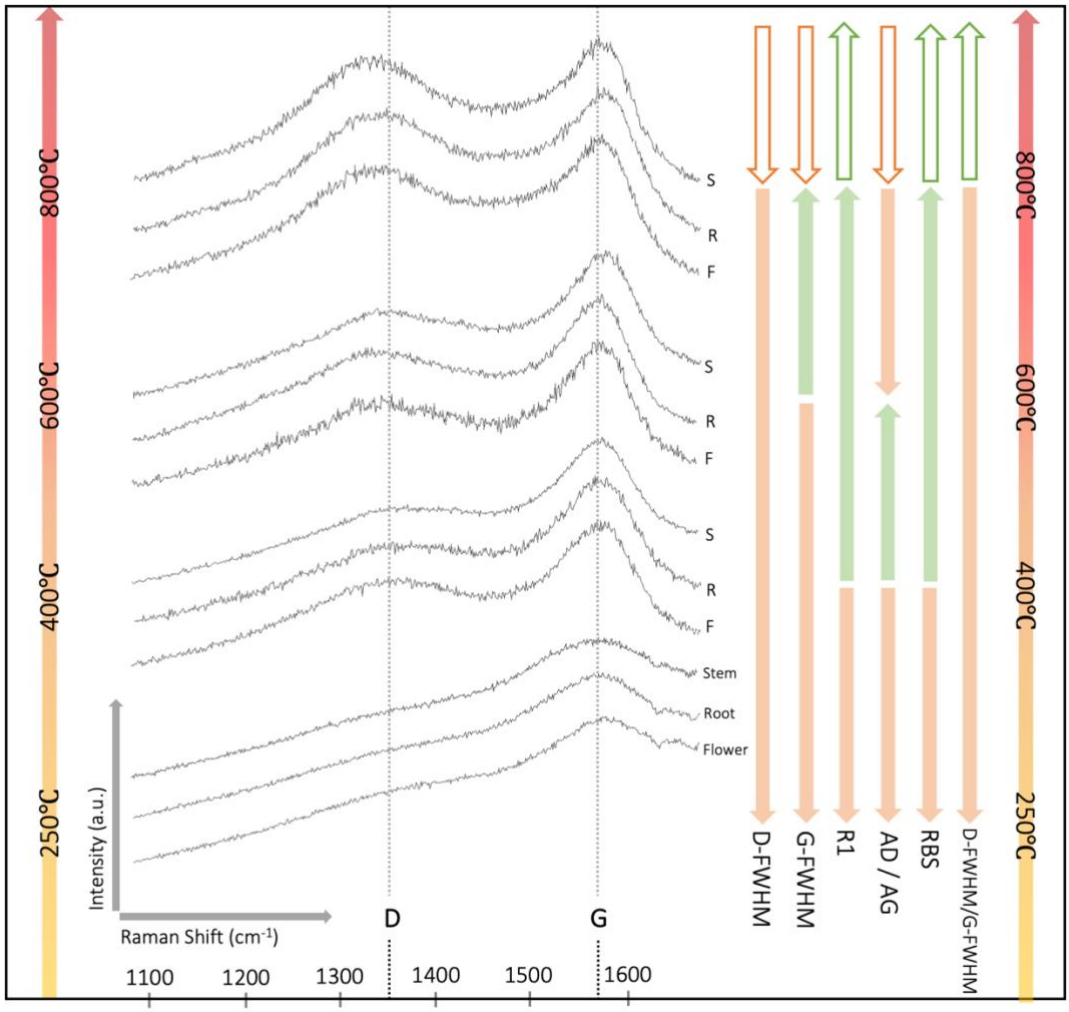

Figure 4. A visual representation of stacked first-order Raman spectra for each temperature, across the three tested materials; roots (R), stems (S) and flowers (F). Relative observed changes in parameters with temperature are also displayed – indicating positive (green arrow), negative (orange arrow), and projected change (outlined arrow) – adapted from Henry et al. (2019b). With increasing formation temperature, visual inspection of spectra indicates width of D- and G-band decreases (narrows) with the exception of 800°C for G-FWHM. The D- and G-band width ratio similarly reduces with temperature – a function of the ratio between components that are simultaneously reducing. RBS, the distance between D- and G-peaks, may be observed in the spectra increasing after 400°C. R1 and AD/AG both show non-linear fluctuating relationships with temperature, though these parameters are less apparent from visual inspection of spectra.

When considering trends in data observed across all components, several significant changes with temperature are apparent. D-FWHM shows a clear reduction with increased temperature, displaying a greater gradient between 250°C and 400°C. G-FWHM similarly reduces from 250-600°C, at which point the data encounters a mild inversion in trend, displaying a gradual increase up to 800°C. R1 shows reduced linearity in the trend, indicating a sharp initial decrease in height ratio from 250-400°C, followed by a small increase from 400-600°C, and a sharp increase up to 800°C. The relationship observed in the trend for AD/AG (band area ratios) is less clear. Whilst the overall trend suggests a reduction in the band area ratio with increased temperature, an inflection point at 600°C suggests a significant change in peak height and width (as the primary components of peak area). This inflection is, however, temporary as AD/AG continues to reduce between 600°C and 800°C. RBS provides the second-most linear parameter relationship, indicating a strong increase with temperature between 400 and 800°C, accompanied by R^2 0.8527. Band width ratio (D-FWHM/G-FWHM) displays inverse proportionality to temperature, although it records little variation in values between 400 and 600°C.

Applying Pearson's correlation coefficient analysis on median trends with temperature (see Figure 5) indicates that the strongest linearity in trend is observed in D-FWHM/G-FWHM, followed by RBS and D-FWHM, whilst moderate to poor linearity is observed in G-FWHM, AD/AG, and R1. However, significance values corresponding to the correlations shown in Figure 5 indicate that none of the parameter trends are statistically significant. This is most likely a function of small sample sizes (n = 4) utilized in these illustrative crossplots, however, all references herein regarding linearity in parameter trends must be considered under the preconception of no statistical significance.

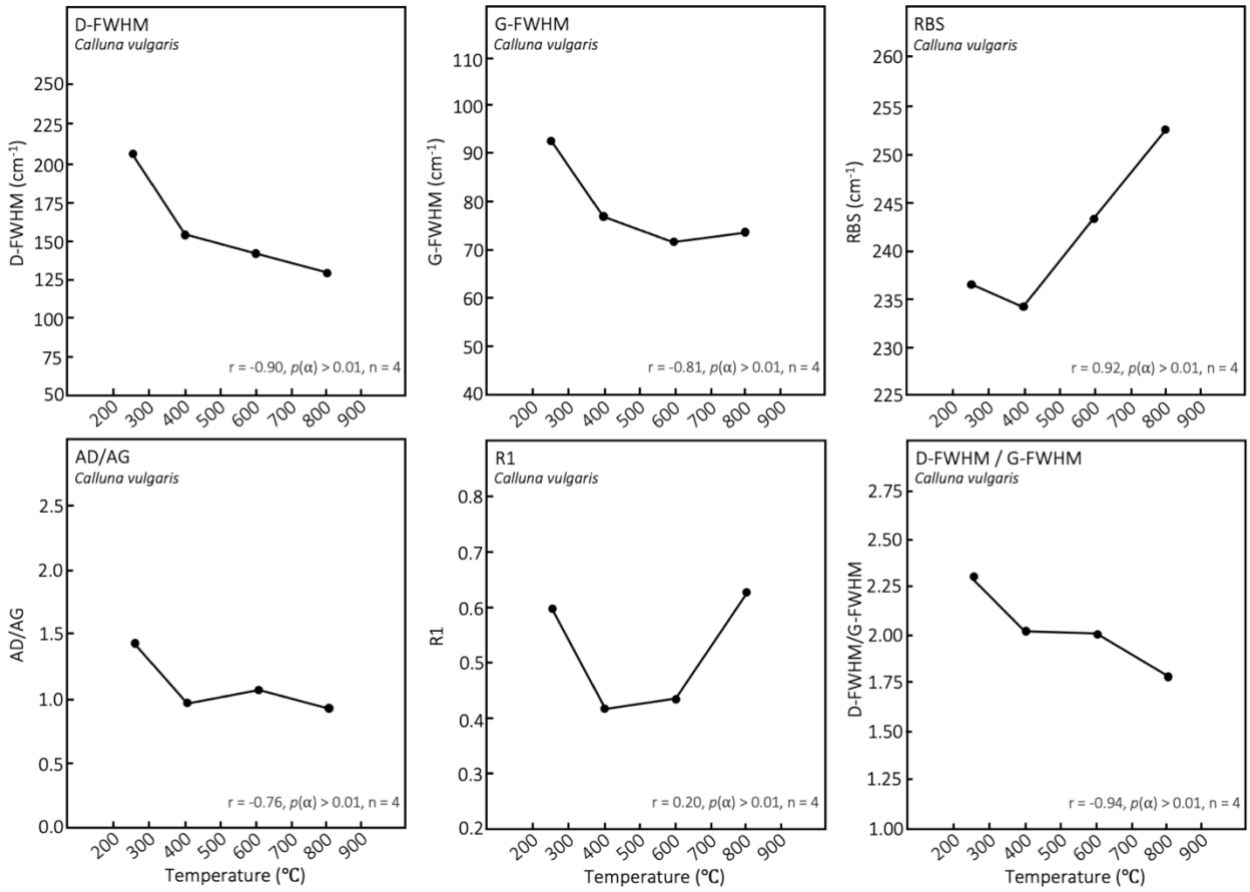

Figure 5. Crossplots displaying the median values for each Raman parameter with increasing charcoal formation temperature. Linearity in trend has been denoted by use of Pearson's correlation coefficient, including corresponding significance, in the bottom right corner of each crossplot. .

Statistical assessment of variation across parameter mean values, according to robust one-way ANOVA testing, suggests all variability in values and their associated trends are statistically significant (Table 2). This is indicated by *p* values below alpha (a) levels 0.05 (95% confidence), with respect to the null hypothesis (Ho). By applying the original and modified Levene's test for homogeneity of variance, we may further infer from $p<0.05$ that median and mean values record heterogenous variance. Unequal variance dictates that we utilise *p*-values from Welch's test of unequal variance (Table 2), indicating a significant difference between mean values across all tested temperatures.

Parameter	One-way ANOVA			Levene's Variance Test	Modified Levene's Test	Welch's Unequal-Variance Test		
	F	*df*	*p*	*p*(mean)	*p*(median)	*F*	*df*	*p*
D-FWHM	600	(3,1730)	<.001	<.001	<.001	808	(3,924)	<.001
G-FWHM	377	(3,1730)	<.001	<.001	<.001	206	(3,893)	<.001
R1	284	(3,1730)	<.001	<.001	<.001	638	(3,871)	<.001
AD/AG	155	(3,1730)	<.001	<.001	<.001	75.3	(3,901)	<.001
RBS	587	(3,1730)	<.001	<.001	<.001	1830	(3,939)	<.001
D-FWHM / G-FWHM	241	(3,1730)	<.001	<.001	<.001	278	(3,936)	<.001

Table 2. Statistical significance of mean values (Welch's *p*) given unequal variance, as determined by the Levene's test for homogeneity of variance and one-way ANOVA analysis. All values have been reported to 3 significant figures.

In order to determine non-parametric pairwise comparisons within parameter variables, given previously determined unequal variance, Games-Howell analysis was utilised (Figure 6). Whilst the majority of comparisons display significance below a0.05, rejecting the aforementioned null, R1 and AD/AG both indicate a single instance of significance >0.05. This indicates that the mean values for R1 at 250°C and 800°C are indistinguishable. The same applies to the AD/AG parameter between 400°C and 800°C. These instances are closely matched to periods of 'inversion' in trends with temperature, as shown in Figure 5.

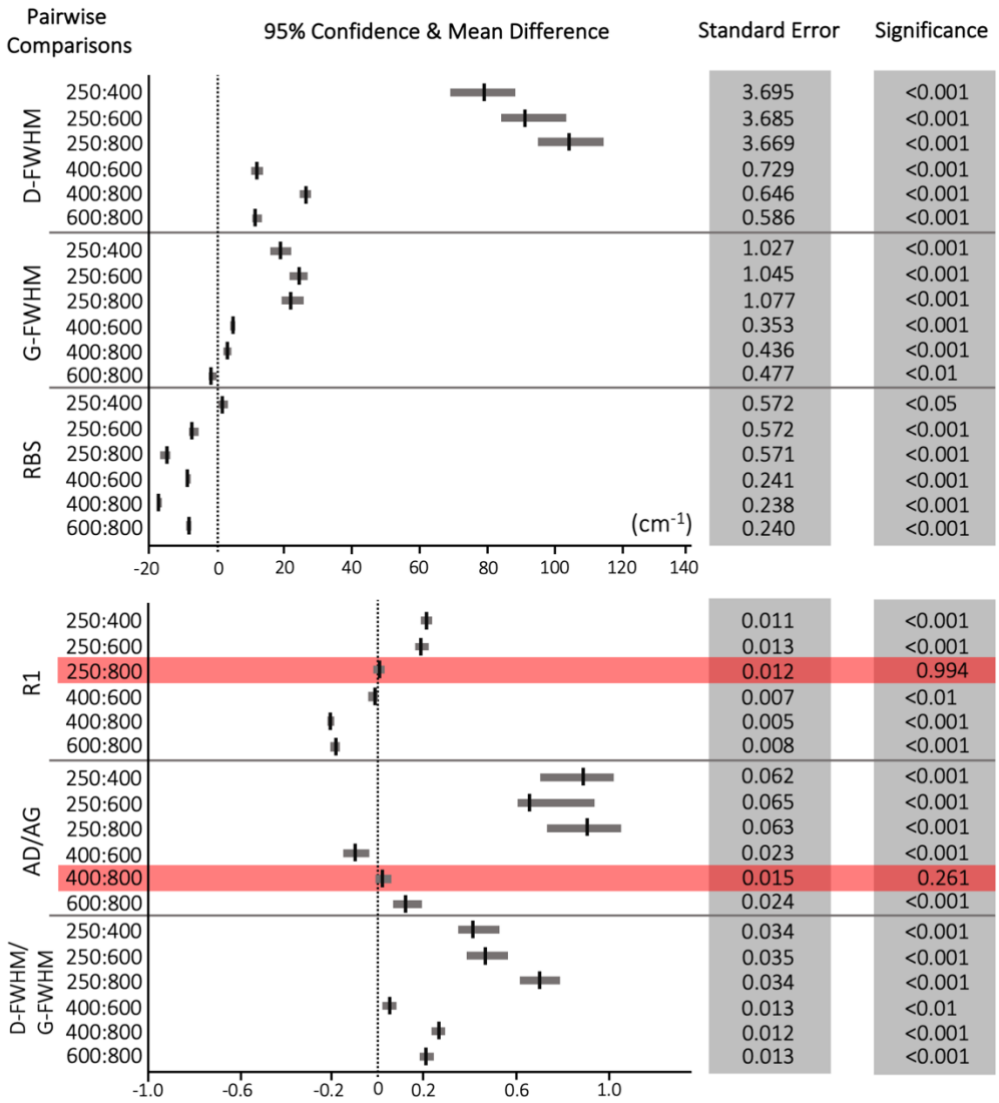

Figure 6. Post-hoc Games-Howell pairwise analysis of mean values across formation temperatures in each tested Raman parameter. The 95% confidence intervals are displayed by grey bars, whilst mean difference values are plotted as black bars. The red highlighted comparison indicates values which are not significant.

3.3 Spectral variability and precursor material

Though the data from different plant components – stems, roots and flowers - remains typically consistent with median trends (Figure 5 and 7), flower results differ most compared to stem and root trends alike. This becomes pronounced particularly across G-FWHM, D-FWHM/G-FWHM and AD/AG parameters, with flower-originated charcoal spectra producing opposite trends between 400 and 800°C. This once again indicates an inversion

point at 600°C within some, but not all, parameters. The lowest apparent variation in material trends occurs in D-FWHM and RBS data. Minor differences are present between stem and root data, manifest in the higher value-frameshifted nature of stem trends compared to root – with the exception of R1, AD/AG and D-FWHM/G-FWHM. This indicates that parameter responses are generally higher for stem charcoal, whilst greater ratio values indicate smaller differences between D- and G-band components. It is also evident that, whilst no consistent pattern is portrayed, parameter data procured from flower charcoal tends to exhibit more instances of high standard deviation compared to stems and roots (Table 3). This suggests a higher degree of variation within flower spectra, respective of formation temperature, and is particularly pronounced in the G-FWHM results.

Parameter	°C	*Calluna* Overall		Flower		Root		Stem	
		Median	*S.D.*	*Median*	*S.D.*	*Median*	*S.D.*	*Median*	*S.D.*
D-FWHM	250	207	77.4	200	74.7	202	64.7	221	87.2
	400	155	11.7	148	9.04	154	7.39	164	10.3
	600	143	10.2	137	12.9	145	7.99	145	5.66
	800	131	6.62	127	8.49	130	4.57	133	14.7
G-FWHM	250	92.6	21.3	96.3	27.3	88.5	9.78	96.0	20.9
	400	76.9	4.42	77.3	4.3	74.0	3.63	79.6	3.65
	600	71.6	6.03	78.2	6.03	67.9	3.73	71.6	2.65
	800	73.6	7.50	74.3	9.99	72.1	5.11	76.3	9.32
R1	250	0.595	0.229	0.612	0.211	0.539	0.223	0.632	0.247
	400	0.416	0.0545	0.406	0.0487	0.444	0.0565	0.403	0.0487
	600	0.434	0.132	0.371	0.0516	0.482	0.202	0.440	0.0416
	800	0.629	0.0878	0.586	0.111	0.653	0.0628	0.629	0.089
AD/AG	250	1.42	1.31	1.25	0.969	1.42	1.30	1.61	1.54
	400	0.962	0.196	0.896	0.206	1.01	0.170	0.976	0.191
	600	1.06	0.445	0.726	0.221	1.27	0.604	1.11	0.143
	800	0.919	0.223	0.826	0.240	0.989	0.208	0.896	0.196
RBS	250	236	11.6	234	15.9	237	6.98	237	9.08
	400	234	3.60	234	3.38	233	3.68	234	3.59
	600	243	3.64	242	4.53	243	3.35	244	2.39
	800	252	3.27	249	3.42	254	1.63	253	27.3
D-FWHM / G-FWHM	250	2.29	0.703	2.09	0.661	2.32	0.692	2.37	0.714
	400	2.02	0.175	1.91	0.155	2.08	0.118	2.07	0.174
	600	2.00	0.214	1.75	0.171	2.13	0.151	2.03	0.0984
	800	1.78	0.162	1.71	0.193	1.81	0.120	1.78	0.127

Table 3. The calculated median and standard deviation (S.D.) values associated with each material Raman dataset, across all Raman parameters at each formation temperature. Highest standard deviations are highlighted. All values have been reported to 3 significant figures.

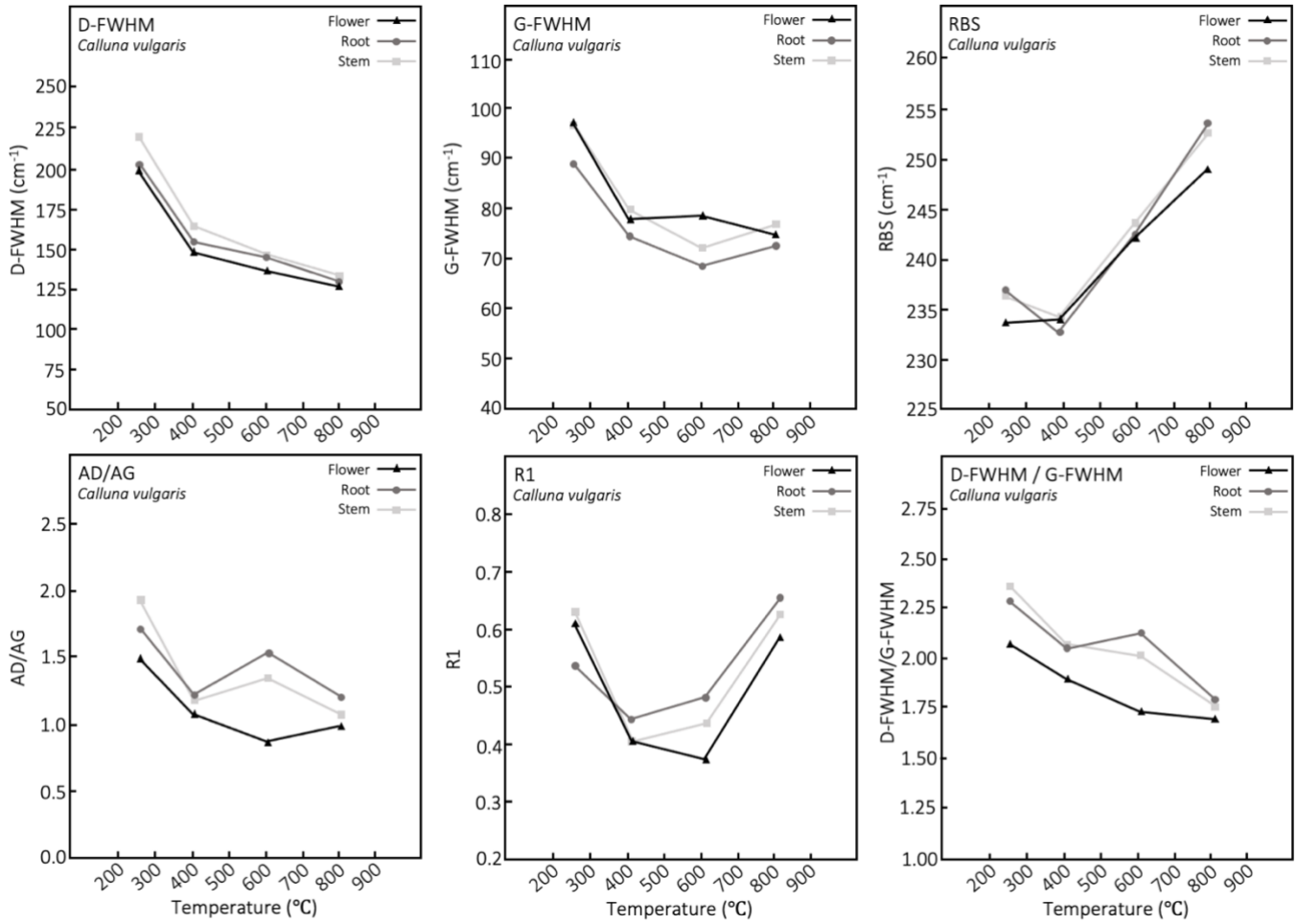

Figure 7. Crossplots displaying temperature-related changes to median parameter values when separated into root, stem and flower components.

4. Discussion

4.1 Raman parameters and temperature

According to Tuinstra and Koenig (1970), our observed reduction in D-FWHM is attributed to increased 'structural arrangement' and lateral growth of graphitic crystallites (L_a) within carbon samples. This was later described as a function of increasing structural order in carbon polyaromatic stacks (Lespade et al., 1982; Paris et al., 2005). Whilst this was shown initially as a product of graphitisation, with charcoal as the lowest denominator of thermal maturity (Tuinstra and Koenig, 1970), later work on carbonised (pyrolysed) wood confirmed the applicability of this trend from 200-1100°C (Yamauchi et al., 2000; Yamauchi and Kurimoto, 2003), 300-1400°C (Paris et al., 2005), 500-1200°C (Ishimaru et al., 2007a; 2007b) and 500-2600°C (Zaida et al., 2007) independently. This parameter has been

correlated directly to structural changes and ordering within wood during carbonisation, noting a correlation between DFWHM as an indicator of 'order' and the growth of polyaromatics, volatilisation of oxygenated functional groups, and destruction of cross-linking structures within amorphous sp^3-bond carbon above 500°C (Ishimaru et al., 2007a; 2007b). Aromatisation, and subsequent development of Raman bands, has been suggested to occur as early as ~300°C (Paris et al., 2005).

G-FWHM has similarly been used to quantify structural order within carbon, as the prime indicator of structural order in sp^2-bonded carbon crystallites (Ferrari and Roberston, 2000; Schito et al., 2017). As with D-FWHM, increasing thermal maturity is accompanied by a similar increase in structural order, thus a decrease in G-FWHM is observed. This trend is, however, notably subtle across studies in charcoal (Yamauchi et al., 2000; Yamauchi and Kurimoto, 2003; Paris et al., 2005; Ishimaru et al., 2007a, 2007b; Sheng, 2007; Zaida et al., 2007). A significant decrease in G-FWHM is presented above 1400°C in Ishimaru et al. (2007b), which in turn is attributed to significant growth of ordered carbon crystallites, and reduction in disordered amorphous sp^2 and sp^3 sites. The change in G-FWHM with temperature has also been directly correlated to changes in charcoal reflectance between 300 and 600°C, indicating an expected reduction as temperature and ordered polyaromatic content increases (Ascough et al., 2010, 2011).

When implemented in the study of charcoal formation under heat treatment, RBS displays a clear increase with temperature up to 700°C (Yamauchi et al., 2000, Yamauchi and Kurimoto, 2003; Paris et al., 2005). Whilst an increase is observed, this is described primarily as the result of a significant shift of the D-band to lower wavelengths, whilst G-band shifts very little to higher wavelengths as graphene sheets compress and merge with temperature (McDonald-Wharry et al., 2013). The predominance of D-band shift during increasing temperature has been described as the result of aromatic ordering (Ferrari and Robertson, 2000; Schito et al., 2017), subsequent crystallite growth (increasing L_a) during aromatisation (Paris et al., 2005) and the removal of amorphous sp^3 carbon from graphene sheets (McDonald-Wharry et al., 2013). The subsequent reduction in RBS at 700°C observed in Yamauchi et al. (2000), Yamauchi and Kurimoto (2003) and Paris et al. (2005) may indicate a similar inflection in the rate of aromatisation at this temperature. Our data, however, does not mirror this inflection beyond 700°C, nor is this observed in additional literature (McDonald-Wharry et al., 2013).

AD/AG displays less application to charcoal within the literature, most likely the result of its complexity – derived from changes in band width and height simultaneously. Yamauchi and Kurimoto (2003) observe an initial reduction in AD/AG from 200-400°C, followed by a sharp increase up to 800°C. This was concluded as the result of increasing proportions of sp^3-bonded amorphous carbon. This would suggest an increase in system disorder up to 800°C, at which point AD/AD and disorder falls again. This trend is consistent with data presented in this paper, although the inflection point is experienced 200°C earlier. Given the suggestion by most parameters that structural order increases with temperature, the conclusion of increased disorder up to 800°C indicates that the complexity of simultaneous height and width changes with temperature may be a more appropriate description of AD/AG results observed.

R1 presents similar complexity. Initially described as inversely proportional to the growth in lateral accretion (L_a) of ordered graphite crystallites, this ratio was similarly deemed inversely proportional to thermal maturity and structural ordering of carbon (Tuinstra and Koenig, 1970). This relationship, however, has since been brought into question, and a significant proportion of research has aimed to implement and construe the relationship between R1 and thermal maturity. Paris et al. (2005) and McDonald-Wharry et al. (2013) note an increase in R1 from ~300-1400°C and 400-1000°C, respectively. These results, according to Tuinstra and Koenig (1970), would indicate a reduction in L_a and subsequent ordering. However, Paris et al. (2005) recorded a simultaneous increase in L_a with temperature – concluding the relationship between L_a and R1 to be more complex than previously considered. Explanation for this trend was later proposed by Zaida et al. (2007), suggesting that crystallites are initially too small for Raman detection. Whilst Zaida et al. (2007) observe an eventual fall in R1 beyond 2000°C, others have observed this fall at much lower temperatures (Yamauchi and Kurimoto, 2003). Such variability in expected and observed trends has been as suggested as a result of applying this ratio to amorphous carbon, given the predominant influence of disorder on both bands at low thermal maturity (Ferrari and Robertson, 2000; Schito et al., 2017). Whilst an increase in R1 is observed above 400°C in the *Calluna* charcoal spectra, an initial fall in values at 250°C suggests further complexity to this relationship. This is countered only with the suggestion that variability is a function of high H and O content, manipulating low temperature aromatisation in wood carbonisation (Paris et al., 2005).

The ratio of D- and G-band widths (D-FWHM/G-FWHM) is not commonly utilised in the study of charcoal under heat treatment, though has been implemented in the study of kerogens under increasing thermal maturity (Schito et al., 2017). In this instance, kerogen samples showed an increase in D-FWHM/G-FWHM with increasing depth and vitrinite reflectance (thermal maturity). This is inconsistent with observed results for *Calluna* charcoal, showing an inverse relationship. It is worth noting, however, that the thermal maturity regime undergone during burial is significantly less intense than heating undergone during a wildfire. The ratio has, ultimately, been related to the reduction in width of the G-band with heating, as aromatic rings within the sample begin to cluster and subsequently 'order' (Ferrari and Robertson, 2000; Schito et al., 2017). Whilst we also observe an initial linear reduction in G-FWHM, Schito et al. (2017) note a simultaneous increase of the D-band width with thermal maturity. Given differences in heating regime of our two studies, resulting in variability in the response of the D-band, this may explain the difference in our recorded trends for D-FWHM/G-FWHM.

Whilst it is evident that comparative studies into the relationship between Raman spectra and charcoal formation are numerous, there are some inconsistencies regarding method of deconvolution. Our application of first-order deconvolution (between 1000 and 2000 cm^{-1}) to D and G bands has been supported by use in similar studies (Tuinstra & Koenig, 1970; Yamauchi et al., 2000; Yamauchi & Kurimoto, 2003; Paris et al., 2005; Mauquoy et al., 2020), and also those focusing on different forms of carbonaceous organic matter (Muirhead et al., 2016, 2017, 2019; Kedar et al., 2020; Schito & Corrado, 2020). In contrast, second order deconvolution (between 2000 and 3500 cm^{-1}) has been deemed inapplicable in amorphous organic matter studies as a function of high fluorescence, obscuring second-order bands (Beyssac et al., 2002). Instances remain where authors have deemed it appropriate in application to pyrolysis (Yamauchi & Kurimoto, 2003; Zaida et al., 2007), though these are few in number. Examples of multi-band first order deconvolution may also be found in the study of charcoal (Yamauchi and Kurimoto, 2003; Ishimaru et al., 2007a, 2007b; Sheng, 2007; McDonald-Wharry et al., 2013), however, the origin and derivation of these additional bands has been deemed controversial (Beyssac et al., 2002; Schito et al., 2017; Schito & Corrado, 2020). Therefore, consideration of the relationship between temperature and charcoal spectra must include the nature of deconvolution processes – though key similarities in principles of parameter change have been highlighted.

4.2 The influence of precursor material

Differences in the Raman spectra when analysing varying material compositions is not unexpected, particularly when considering the chemical changes undergone during the pyrolysis of plant material. According to Ishimaru et al. (2007a), the proportion of cellulose in plant material significantly impacts structural ordering with pyrolysis, greatly influenced by the greater ratio of O/C reported in cellulose (Byrne and Nagle, 1997). Experiments assessing the spectra of isolated cellulose, lignin, and wood (a mixture of hemicellulose, cellulose and lignin) have determined structural order within samples increased across cellulose-wood-lignin, given lignin displays the lowest FWHM values (Ishimaru et al., 2007a). Though trends between the materials were somewhat dissimilar, wood and cellulose were most alike, suggesting cellulose content provides the greatest limitation to structural ordering. Potential impacts of this are highlighted further when considering the increase in lignin observed in plant material as it matures, and natural variation in biochemistry both between and within a species.

Given the prominence of vascular tissue in root and stem material, and its dependence on structurally supportive lignin structures, it would be expected that this material under Raman spectroscopy would exhibit lower FWHM values than cellulose-dominant flower material. This, however, is not entirely the case in the *Calluna* charcoal spectra. Whilst root material displays lower G-FWHM values, suggesting greater structural order at each temperature, stem and flower material fluctuate in intensity. Contrary to this, D-FWHM consistently exhibits lower values in flower material. Though such differences are notable, stem and root materials do exhibit similar trends in FWHM analysis. This perhaps suggests that, though the data reported in Ishimaru et al. (2007a) may not be applicable to wider proportional trends in plant material, there are differences in the impact of material on Raman results. An experimental analysis of cellulose and lignin proportions within the tested materials is required to understand this relationship further.

It appears that the content of cellulose may further impact spectra observed at lower temperatures, at the onset of aromatisation. Yamauchi and Kurimoto (2003) record significant jumps in trend between 200°C and 300°C, not dissimilar from results presented in

this study. In contrast, however, they record clear spectra at 200°C, whereas the spectra in this study were of limited quality at 250°C, accompanied by a poor degree of charcoalification in samples. Whilst this may be a function of dwell time impacting extent of sample pyrolysis, previous works discussed in Yamauchi et al. (2000) note the differences in aromatisation thresholds for structural components in wood; hemicellulose degrades at 200-250°C, cellulose at 240-350°C, and lignin at 280-500°C (Graham et al., 1984). This is pertinent when considering potential differences in reported aromatisation thresholds for varied material.

4.3 Thermal maturation in similar organics

The study of coal and thermal maturity utilising Raman spectroscopy has, historically, been linked to the study of charcoal during heat treatment in an extensive review by Potgieter-Vermaak et al. (2011). This relationship is no doubt perpetuated by similarities in vegetative origin, interrelation with combustion, and the presence of wildfire-derived charcoal macerals within coals. Therefore, the parameters used in understanding coal maturation – the response of plant material to heat – pertains to the understanding of charcoal. Initial research into Raman and coal determined that study of the D-band width was most applicable in assessing low-grade coals, given their disordered nature (Wopenka and Pasteris, 1993; Quirico et al., 2005), congruent with our assessment that changes to the spectra with heating are most prominent in the D-band. Later work, however, deemed the sensitivity of Raman parameters to the bulk assessment of coal maturity to be dependent on the thermal maturity itself (Quirico et al., 2005). It was identified that whilst D-FWHM and R1 (ID/IG) are most sensitive to higher maturities - between 3% and 7% Ro – changes to the width of the G-band was better suited to low-medium grade coals (1-5% Ro). Quirico et al. (2005) also identified an initial fall in R1 with maturity, followed by an inversion in at 5% Ro, which may correspond to the inversion observed in the *Calluna* charcoal spectra. This is, however, deemed indicative of the inapplicability of R1 to poorly ordered amorphous organic material (Quirico et al., 2005; Li, 2007). Subsequent work utilising UV-Raman has also shown little correlation between maturity and D-FWHM in mature coals, and R1 in immature coals, whilst G-FWHM shows an inverse non-linear relationship with maturation (Quirico et al., 2020). This contradicts earlier research, with data indicating a linear inverse relationship – as observed in the current work – between maturity and D-FWHM, and G-FWHM,

respectively (Hinrichs et al., 2014; Zhang and Li, 2019). Zhang and Li (2019) have further iterated the highly linear positive relationship between RBS and maturity, though in agreement with Quirico et al. (2005), note the requirement for utilising different parameters under different maturities.

It has, however, been proposed that most studies are reliant on bulk analysis of coals, without consideration of the extreme heterogeneity exhibited between coal macerals (Guedes et al., 2010). Analysis of the maturation of collotelinite, fusinite and macrinite has indicated that the macerals, alongside bulk analysis, exhibit a related decrease in G-FWHM and increase in R1 (Guedes et al., 2010). Further still, similarities between collotelinite and bulk macerals indicate its suitability at assessing overall thermal maturity, whereas fusinite and macrinite share similarity in Raman response given their shared oxidative formation pathway. This consideration of internal sample heterogeneity remains poignant given the variability in Raman data we have observed between charcoals of differing precursor materials (Figure 7).

4.4 Assessing wildfire intensity

Following the experimental analysis of Raman spectroscopic parameters with increasing heat treatment, it can be established that the assessment of wildfire intensity benefits from the use of particular parameters. This is alongside an established understanding of structural changes in fossil plant material with maturation, namely coal and charcoal. Our results indicate that the parameter with the most linear apparent trend with increasing temperature of formation remains D-FWHM/G-FWHM (Figure 5). Though seldom applied in the analysis of organic material, this parameter benefits from the application and consideration of both spectral bands, D and G. This ensures the assessment of thermal maturity in fossil charcoal samples incorporates changes in both disordered structures, and ordered graphitic crystallites (Tuinstra and Koenig, 1970). Linearity with temperature change ensures any assessment of intensity is not impeded by inversions as identified in other parameters. The nature of D-FWHM/G-FWHM as a ratio also increases the applicability of this parameter to comparison studies – ensuring variable datasets are comparable, and concepts transferable. This is, however, contrasted by previous determination that this parameter may be inherently impacted by multi-band deconvolution, limiting comparability across studies of variable methodology.

Though exhibiting lower apparent linearity with temperature, sole analysis of intensity utilising D-FWHM offers further benefits. Homogeneity in the spectral response between all component materials (Figure 7) indicates that D-FWHM trends with temperature are mostly unaffected by the composition of sampled charcoal. Further still, D-FWHM has no reliance on changes to the G-band, which does not indicate a linear trend with temperature. This lack of consideration for G-band changes may contradict prior applications (Yamauchi et al., 2000; Yamauchi and Kurimoto, 2003; Paris et al., 2005; Quirico et al., 2005; Ishimaru et al., 2007a, 2007b; Sheng, 2007; Zaida et al., 2007; Hinrichs et al., 2014; Zhang and Li, 2019) though it offers a method of circumventing a significant dilemma when assessing the thermal maturity of palaeocharcoals using Raman – oxidation. Most palaeofire research in tandem with Raman has focused primarily on the impact of diagenetic alteration on charcoal microstructure. Cohen-Ofri et al. (2006) identified that fossil charcoals (40,000 BP) display a higher proportion of disorganised material in their structure due to the oxidative humification of graphitic material. The selective preservation of more disordered material has also been suggested as a function of the physical instability of more-graphitic materials, preferentially removed by water (Inoue et al., 2017). This concept was countered somewhat by de Sousa et al. (2020), who recently identified changes in archaeological biochar microstructure with soil depth - reporting an initial alteration period of 2000 years within the amorphous charcoal structures. Whilst the succeeding 9000 years of preservation lead to an increase in oxidative alteration of graphitic microstructures, it was not as intense as changes seen in the amorphous material. By applying D-FWHM and avoiding G-band analyses, skewed assumptions of maturation due to changes in graphitic material during diagenesis may be counteracted. Limitation in the application of D-FWHM does, however, reside in the aforementioned impact of multi-band deconvolution. Changes in width values as a result of multi-band deconvolution may in turn limit the comparability of datasets and applicability of precise geothermometry. Palaeofire intensity change derived as a function of relative D-FWHM change appears to remain robust regardless of deconvolution process.

Whilst RBS also displays high apparent linearity in trend with temperature, its use in assessing wildfire temperature and intensity is hindered by the inversion between 250°C and 400°C, which may make the differentiation of low-temperature smoldering fires inaccurate. Further work is required in this respect to determine the exact threshold between these

temperatures at which the inversion occurs, to better constrain the applicability of this parameter. This complication is also attributable to R1, AD/AG and G-FWHM, making their use in assessing wildfire intensity complex and potentially problematic. Whilst this may appear to suggest that the use of these parameters is entirely null, there are means by which this is counteracted. Mauquoy et al. (2020), in the first extensive study into wildfire intensity and Raman spectroscopy, utilised R1 under assumed linearity concordant with the majority of prior Raman-charcoal study (e.g. Paris et al., 2005; Zaida et al., 2007; McDonald-Wharry et al., 2013). This was, however, in conjunction with a qualitative visual analysis of spectra. Whilst we have observed disparity in data at 250°C, leading to non-linearity, the spectra at this temperature are distinct and allow for clear differentiation between low and high temperatures (Figure 4). Therefore, with respect to Mauquoy et al. (2020), the assessment of wildfires using R1 is justified, but only alongside the consideration of individual spectra. This method, however, may not feasible when considering extensive successions of charcoal samples and accompanying datasets.

A further key consideration, with reference to all parameters, is the nature of the applicability of Raman when analysing charcoals derived from material other than *Calluna vulgaris*. Whilst our experimental assessment of *Calluna* charcoals has yielded results comparable in nature to those gathered in prior literature (see Section 4.1 and 4.3) our conclusions regarding the potential impact of variable biochemistry (see Section 4.2) suggest the need for further experimental study into charcoals derived from other species.

5. Conclusions

Raman spectroscopy represents an efficient and non-destructive method of characterising the structural changes associated with charcoal formation. This study has produced a range of comparable parameters that indicate structure in *Calluna* charcoal is dictated primarily by changes to D-band and associated structural disorder. As temperature of formation increases, *Calluna* charcoal exhibits a strong inverse proportionality in structural ordering within D-FWHM and D-FWHM/G-FWHM parameters. However, multi-dependent parameters such as intensity (R1) and area (AD/AG) ratios portray more complex relationships. This complexity is heightened by variation in results between different origin materials. Whilst previous research has reported on the differences between wood components and structural ordering as a function of cellulose and lignin content, this

relationship has been shown to grow more complex when attributed to broader material classification. In order to assess changes in wildfire intensity, as a function of charcoal pyrolysis temperature, we have determined that the most effective parameters are D-band width (D-FWHM) and the ratio of D and G-band width (D-FWHM/G-FWHM). Whilst D-FWHM/G-FWHM indicates the greatest apparent linearity with temperature and incorporates changes in both D- and G-bands, the impact of oxidation on graphitic material during diagenesis is still under discussion. Therefore, given uncertainty over the impact of the G-band in the band-width ratio (D-FWHM/G-FWHM), instances of unknown diagenetic influence would benefit from sole D-FWHM application. The application of these parameters must, however, be considerate of variability in derived parameters as a function of the Raman deconvolution process.

Further research is required to determine the proportion of cellulose and lignin in different plant materials, within and between species, and the influence this displays on spectroscopic trends. Additionally, further experimental work is required to refine and evaluate the influence of pyrolysis methodology, moisture and heat flux on charcoal structure and the subsequent Raman data. Nevertheless, the application of Raman to experimental charcoals has revealed significant insight into the applicability of certain parameters, considered otherwise comparable in the study of thermal maturity in organic carbons. Ultimately, Raman spectroscopy is an unexplored method of characterising palaeowildfires, with extensive potential.

Acknowledgments

We would like to thank Maria-Ara Carballo-Meilan, Ilse Kamerling and Colin Taylor for their kind assistance with the procurement and operation of pyrolysis equipment. The use of *Calluna vulgaris* material in this study was informed under an assessment of 'least concern' by the *IUCN Red List of Threatened Species*. This research was supported by funds from the School of Geosciences, University of Aberdeen.

Data Availability

All data appropriate to the conclusions of this study have been stored in *Zenodo* data repository, under temporary restricted access. Access is currently permitted for manuscript reviewers at https://doi.org/10.5281/zenodo.4191885. This dataset will be made available

References

Abu Hamad, A. M. B., Jasper, A., & Uhl, D. (2012). The record of Triassic charcoal and other evidence for palaeo-wildfires: Signal for atmospheric oxygen levels, taphonomic biases or lack of fuel? *International Journal of Coal Geology*, 96-97, 60-71. https://doi.org/10.1016/j.coal.2012.03.006

Ascough, P., Bird, M., Francis, S. M., Thornton, B., Midwood, A. J., Scott, A. C., & Apperley, D. (2011). Variability in oxidative degradation of charcoal: Influence of production conditions and environmental exposure. *Geochimica et Cosmochimica Acta*, 75(9), 2361-2378. https://doi.org/10.1016/j.gca.2011.02.002

Ascough, P. L., Bird, M. I., Scott, A. C., Collinson, M. E., Cohen-Ofri, I., Snape, C. E., & Le Manquais, K. (2010). Charcoal reflectance measurements: implications for structural characterization and assessment of diagenetic alteration. *Journal of Archaeological Science*, 37(7), 1590-1599. https://doi.org/10.1016/j.jas.2010.01.020

Belcher, C. M., & Hudspith, V. A. (2016). The formation of charcoal reflectance and its potential use in post-fire assessments. *International Journal of Wildland Fire*, 25(7), 775-779. https://doi.org/10.1071/WF15185

Benicio, J. R. W., Jasper, A., Spiekermann, R., Garavaglia, L., Pires-Oliveira, E. F., Machado, N. T. G., & Uhl, D. (2019). Recurrent palaeo-wildfires in a Cisuralian coal seam: A palaeobotanical view on high-inertinite coals from the Lower Permian of the Paraná Basin, Brazil. *PLoS ONE*, 14(3), e0213854. https://doi.org/10.1371/journal.pone.0213854

Beyssac, O., Goffé, B., Chopin, C., & Rouzaud, J. (2002). Raman spectra of carbonaceous material in metasediments: a new geothermometer. *Journal of Metamorphic Geology*, 20(9), 859-871. https://doi.org/10.1046/j.1525-1314.2002.00408.x

Bojesen-Koefoed, J. A., Petersen, H. I., Surlyk, F., & Vosgerau, H. (1997). Organic petrography and geochemistry of inertinite-rich mudstones, Jakobsstigen Formation, Upper Jurassic, northeast Greenland: Indications of forest fires and variations in

relative sea-level. *International Journal of Coal Geology*, 34(3-4), 345-370. https://doi.org/10.1016/S0166-5162(97)00030-X

Butler, B. W., Cohen, J., Latham, D. J., Schuette, R. D., Sopko, P., Shannon, K. S., et al. (2004). Measurements of radiant emissive power and temperatures in crown fires. *Canadian Journal of Forest Research*, 34(8), 1577-1587. https://doi.org/10.1139/x04-060

Byrne, C. E., & Nagle, D. C. (1997). Carbonized wood monoliths—Characterization. *Carbon*, 35(2), 267-273. https://doi.org/10.1016/S0008-6223(96)00135-2

Cardoso, D. S., Mizusaki, A. M. P., Guerra-Sommer, M., Menegat, R., Barili, R., Jasper, A., & Uhl, D. (2018). Wildfires in the Triassic of Gondwana Paraná Basin. *Journal of South American Earth Sciences*, 82, 193-206. https://doi.org/10.1016/j.jsames.2017.12.018

Cohen-Ofri, I., Weiner, L., Boaretto, E., Mintz, G., & Weiner, S. (2006). Modern and fossil charcoal: aspects of structure and diagenesis. *Journal of Archaeological Science*, 33(3), pp. 428-439. https://doi.org/10.1016/j.jas.2005.08.008

Davis, K.P. (1959). *Forest Fire, Control and Use*. New York: McGraw-Hill.

Diessel, C. F. K. (2010). The stratigraphic distribution of inertinite. *International Journal of Coal Geology*, 81(4), 251-268. https://doi.org/10.1016/j.coal.2009.04.004

Drysdale, D. (1998). *An Introduction To Fire Dynamics* (2nd Ed.). Chichester, UK: John Wiley & Sons.

Edwards D., & Axe L. (2004). Anatomical evidence in the detection of the earliest wildfires. *PALAIOS*, 19(2), 113-128. https://doi.org/10.1669/0883-1351(2004)019<0113:AEITDO>2.0.CO;2

Ferrari, A. C., & Robertson, J. (2000). Interpretation of Raman spectra of disordered and amorphous carbon. *Physical Review B*, 61(20), 14095-14107. https://doi.org/10.1103/PhysRevB.61.14095

Glasspool, I. J. (2000). A major fire event recorded in the mesofossils and petrology of the Late Permian, Lower Whybrow coal seam, Sydney Basin, Australia. *Palaeogeography, Palaeoclimatology, Palaeoecology*, 164(1-4), 357-380. https://doi.org/10.1016/S0031-0182(00)00194-2

Glasspool, I. J., Edwards, D. and Axe, L. (2004). Charcoal in the Silurian as evidence for the earliest wildfire. *Geology*, 32(5), p. 381-383. https://doi.org/10.1130/G20363.1

Glasspool, I. J., Edwards, D., & Axe, L. (2006). Charcoal in the Early Devonian: A wildfire-derived Konservat–Lagerstätte. *Review of Palaeobotany and Palynology*, 142(3-4), 131-136. https://doi.org/10.1016/j.revpalbo.2006.03.021

Graham, R. G., Bergougnou, M. A., & Overend, R. P. (1984). Fast pyrolysis of biomass. *Journal of Analytical and Applied Pyrolysis*, 6(2), 95–135. https://doi.org/10.1016/0165-2370(84)80008-X

Guedes, A., Valentim, B., Prieto, A. C., Rodrigues, S., & Noronha, F. (2010). Micro-Raman spectroscopy of collotelinite, fusinite and macrinite. *International Journal of Coal Geology*, 83(4), 415-422. https://doi.org/10.1016/j.coal.2010.06.002

Henry, D. G., Jarvis, I., Gillmore, G., & Stephenson, M. (2019a). A rapid method for determining organic matter maturity using Raman spectroscopy: Application to Carboniferous organic-rich mudstones and coals. *International Journal of Coal Geology*, 203, 87-98. https://doi.org/10.1016/j.coal.2019.01.003

Henry, D. G., Jarvis, I., Gillmore, G., & Stephenson, M. (2019b). Raman spectroscopy as a tool to determine the thermal maturity of organic matter: Application to sedimentary, metamorphic and structural geology. *Earth-Science Reviews*, 198, 102936. https://doi.org/10.1016/j.earscirev.2019.102936

Henry, D. G., Jarvis, I., Gillmore, G., Stephenson, M., & Emmings, J. F. (2018). Assessing low-maturity organic matter in shales using Raman spectroscopy: Effects of sample preparation and operating procedure. *International Journal of Coal Geology*, 191, 135-151. https://doi.org/10.1016/j.coal.2018.03.005

Hinrichs, R., Brown, M. T., Vasconcellos, M. A. Z., Abrashev, M. V., & Kalkreuth, W. (2014). Simple procedure for an estimation of the coal rank using micro-Raman spectroscopy. *International Journal of Coal Geology*, 136, 52-58. https://doi.org/10.1016/j.coal.2014.10.013

Hudspith, V. A., & Belcher, C. M. (2017). Observations of the structural changes that occur during charcoalification: Implications for identifying charcoal in the fossil record. *Palaeontology*, 60(4), 503–510. https://doi.org/10.1111/pala.12304

Hudspith, V. A., Belcher, C. M., Kelly, R., & Hu, F. S. (2015). Charcoal reflectance reveals early Holocene boreal deciduous forests burned at high intensities. *PLOS One*, 10(4), e. 0120835. https://doi.org/10.1371/journal.pone.0120835

Hudspith, V. A., Belcher, C. M., & Yearsley, J. M. (2014). Charring temperatures are driven by the fuel types burned in a peatland wildfire. *Frontiers in Plant Science*. https://doi.org/10.3389/fpls.2014.00714

Inoue, J., Yoshie, A., Tanaka, T., Onji, T., & Inoue, Y. (2017). Disappearance and alteration process of charcoal fragments in cumulative soils studied using Raman spectroscopy. *Geoderma*, 285, 164-172. https://doi.org/10.1016/j.geoderma.2016.09.032

Ishimaru, K., Hata, T., Bronsveld, P., Meier, D., & Imamura, Y. (2007a). Spectroscopic analysis of carbonization behaviour of wood, cellulose and lignin. *Journal of Materials Science*, 42, 122-129. https://doi.org/10.1007/s10853-006-1042-3

Ishimaru, K., Hata, T., Bronsveld, P., Nishizawa, T., & Imamura, Y. (2007b). Characterization of sp2- and sp3 bonded carbon in wood charcoal. *Journal of Wood Science*, 53, 442-448. https://doi.org/10.1007/s10086-007-0879-7

Jasper, A., Guerra-Sommer, M., Abu Hamad, A. M. B., Bamford, M., Bernardes-de-Oliveira, M. E. C., Tewari, R., & Uhl, D. (2013). The burning of Gondwana: Permian fires on the southern continent - A palaeobotanical approach. *Gondwana Research*, 24(1), 148-160. https://doi.org/10.1016/j.gr.2012.08.017

Jones, T. P., Scott, A. C., & Cope, M. (1991). Reflectance measurements and the temperature of formation of modern charcoals and implications for studies of fusain. *Bulletin de la Societe Geologique de France*, 162(2), 193-200.

Jorio, A., Ribeiro-Soares, J., Cançado, L. G., Falcão, N. P. S., Dos Santos, H. F., Baptista, D. L., et al. (2012). Microscopy and spectroscopy analysis of carbon nanostructures in highly fertile Amazonian anthrosoils. *Soil and Tillage Research*, 122, 61-66. https://doi.org/10.1016/j.still.2012.02.009

Kedar, L., Bond, C., & Muirhead, D. (2020). Carbon ordering in an aseismic shear zone: Implications for Raman geothermometry and strain tracking. *Earth and Planetary Science Letters*, 549, 116536. https://doi.org/10.1016/j.epsl.2020.116536

Lespade, P., Al-Jishi, R., & Dresselhaus, M. S. (1982). Model for Raman scattering from incompletely graphitized carbons. *Carbon*, 20(5), 427-431. https://doi.org/10.1016/0008-6223(82)90043-4

Li, C-Z. (2007). Some recent advances in the understanding of the pyrolysis and gasification behaviour of Victorian brown coal. *Fuel*, 86(12-13), 1664-1683. https://doi.org/10.1016/j.fuel.2007.01.008

Lünsdorf, N. (2016). Raman spectroscopy of dispersed vitrinite — Methodical aspects and correlation with reflectance. *International Journal of Coal Geology*, 153, 75-86. https://doi.org/10.1016/j.coal.2015.11.010

Marynowski, L., Scott, A. C., Zatoń, M., Parent, H., & Garrido, A. C. (2011). First multi-proxy record of Jurassic wildfires from Gondwana: Evidence from the Middle Jurassic of the Neuquén Basin, Argentina. *Palaeogeography, Palaeoclimatology, Palaeoecology*, 299(1-2), 129-136. https://doi.org/10.1016/j.palaeo.2010.10.041

Mastrolonardo, G., Francioso, O., Di Foggia, M., Bonora, S., Rumpel, C., & Certini, G. (2014). Application of thermal and spectroscopic techniques to assess fire-induced changes to soil organic matter in a Mediterranean forest. *Journal of Geochemical Exploration*, 143, 174-182. https://doi.org/10.1016/j.gexplo.2014.04.010

Mauquoy, D., Payne, R. J., Babeshko, K. V., Bartlett, R., Boomer, I., Bowey, H., et al. (2020). Falkland Island peatland development processes and the pervasive presence of fire. *Quaternary Science Reviews*, 240, 106391. https://doi.org/10.1016/j.quascirev.2020.106391

McDonald-Wharry, J., Manley-Harris, M., & Pickering, K. (2013). Carbonisation of biomass-derived chars and the thermal reduction of a graphene oxide sample studied using Raman spectroscopy. *Carbon*, 59, 383-405. https://doi.org/10.1016/j.carbon.2013.03.033

McParland, L. C., Collinson, M. E., Scott, A. C., & Campbell, G. (2009). The use of reflectance values for the interpretation of natural and anthropogenic charcoal assemblages. *Archaeological and Anthropological Sciences*, 1, 249-261. https://doi.org/10.1007/s12520-009-0018-z

McParland, L. C., Collinson, M. E., Scott, A. C., Steart, D. C., Grassineau, N. V., & Gibbons, S. J. (2007). Ferns and fires: Experimental charring of ferns compared to wood and implications for paleobiology, paleoecology, coal petrology, and isotope geochemistry. *PALAIOS*, 22, 528-538. https://doi.org/10.2110/palo.2005.p05-138r

Menning, K. M., & Stephens, S. L. (2007). Fire Climbing in the Forest: A Semiqualitative, Semiquantitative Approach to Assessing Ladder Fuel Hazards. *Western Journal of Applied Forestry*, 22(2), 88-93. https://doi.org/10.1093/wjaf/22.2.88

Muirhead, D. K., Bond, C. E., Watkins, H., Butler, R. W. H., Schito, A., Crawford, Z., & Marpino, A. (2019). Raman spectroscopy: an effective thermal marker in low temperature carbonaceous fold–thrust belts. *Geological Society, London, Special Publications*, 490, 135-151. https://doi.org/10.1144/SP490-2019-27

Muirhead, D., Bowden, S., Parnell, J., & Schofield, N. (2017). Source rock maturation owing to igneous intrusion in rifted margin petroleum systems. *Journal of the Geological Society*, 174(6), 979-987. https://doi.org/10.1144/jgs2017-011

Muirhead, D. K., Parnell, J., Spinks, S., & Bowden, S. A. (2016). Characterization of organic matter in the Torridonian using Raman spectroscopy. *Geological Society, London, Special Publications*, 448, 71-80. https://doi.org/10.1144/SP448.2

Muirhead, D. K., Parnell, J., Taylor, C., & Bowden, S. A. (2012). A kinetic model for the thermal evolution of sedimentary and meteoritic organic carbon using Raman spectroscopy. *Journal of Analytical and Applied Pyrolysis*, 96, 153-161. https://doi.org/10.1016/j.jaap.2012.03.017

Orvis, K. H., Lane, C. S., & Horn, S. P. (2005). Laboratory production of vouchered reference charcoal from small wood samples and non-woody plant tissues. *Palynology*, 29(1), 1-11.

Paris, O., Zollfrank, C., & Zickler, G. A. (2005). Decomposition and carbonisation of wood biopolymers—a microstructural study of softwood pyrolysis. *Carbon*, 43(1), 53-66. https://doi.org/10.1016/j.carbon.2004.08.034

Petersen, H. I., & Lindström, S. (2012). Synchronous wildfire activity rise and mire deforestation at the Triassic–Jurassic boundary. *PLoS ONE*, 7(10), e47236. https://doi.org/10.1371/journal.pone.0047236

Potgieter-Vermaak, S., Maledi, N., Wagner, N., Van Heerden, J. H. P., Van Grieken, R., & Potgieter, J. H. (2011). Raman spectroscopy for the analysis of coal: a review. *Journal of Raman Spectroscopy*, 42(2), 123-129. https://doi.org/10.1002/jrs.2636

Pyne, S., Andrews, P., & Laven, R. (1996). *Introduction to Wildland Fire - Fire Management in the United States*. New York: Wiley.

Quirico, E., Bonal, L., Montagnac, G., Beck, P., & Reynard, B. (2020). New insights into the structure and formation of coals, terrestrial and extra-terrestrial kerogens from resonant UV Raman spectroscopy. *Geochimica et Cosmochimica Acta*, 282, 156-176. https://doi.org/10.1016/j.gca.2020.05.028

Quirico, E., Rouzaud, J-N., Bonal, L., & Montagnac, G. (2005). Maturation grade of coals as revealed by Raman spectroscopy: Progress and problems. *Spectrochimica Acta Part A: Molecular and Biomolecular Spectroscopy*, 61(10), 2368-2377. https://doi.org/10.1016/j.saa.2005.02.015

Rein, G. (2013). Smouldering fires and natural fuels. In C. M. Belcher (Ed.), *Fire phenomena and the Earth system: An interdisciplinary guide to fire science* (pp. 15-33). Oxford, UK: John Wiley & Sons.

Rein G. (2016). Smoldering Combustion. In M. J. Hurley, et al. (Eds.), *SFPE Handbook of Fire Protection Engineering* (pp. 581-603). New York, NY: Springer.

Rein, G., Cleaver, N., Ashton, C., Pironi, P., & Torero, J. L. (2008). The severity of smouldering peat fires and damage to the forest soil, *Catena*, 74(3), 304-309. https://doi.org/10.1016/j.catena.2008.05.008

Ribeiro-Soares, J., Cançado, L. G., Falcão, N. P. S., Martins Ferreira, E. H., Achete, C. A., & Jorio, A. (2012). The use of Raman spectroscopy to characterize the carbon materials found in Amazonian anthrosoils. *Journal of Raman Spectroscopy*, 44(2), 283-289. https://doi.org/10.1002/jrs.4191

Rimmer, S. M., Hawkins, S. J., Scott, A. C., & Cressler, W. L. (2015). The rise of fire: Fossil charcoal in late Devonian marine shales as an indicator of expanding terrestrial ecosystems, fire, and atmospheric change. *American Journal of Science*, 315(8), 713-733. https://doi.org/10.2475/08.2015.01

Rundel P.W. (1981). Fire as an Ecological Factor. In O. L. Lange, P. S. Nobel, C. B. Osmond, H. Ziegler (Eds.), *Physiological Plant Ecology I. Encyclopedia of Plant Physiology* (Vol. 12/A, pp. 501-528). Heidelberg, Berlin: Springer.

Schito, A., & Corrado, S. (2020). An automatic approach for characterization of the thermal maturity of dispersed organic matter Raman spectra at low diagenetic stages. *Geological Society, London, Special Publications*, 484, 107-119. https://doi.org/10.1144/SP484.5

Schito, A., Romano, C., Corrado, S., Grigo, D., & Poe, B. (2017). Diagenetic thermal evolution of organic matter by Raman spectroscopy. *Organic Geochemistry*, 106, 57-67. https://doi.org/10.1016/j.orggeochem.2016.12.006

Scott, A. C. (1989). Observations on the nature and origin of fusain. *International Journal of Coal Geology*, 12(1-4), 443-475. https://doi.org/10.1016/0166-5162(89)90061-X

Scott, A. C. (2000). The Pre-Quaternary history of fire. *Palaeogeography, Palaeoclimatology, Palaeoecology*, 164(1-4), 281-329. https://doi.org/10.1016/S0031-0182(00)00192-9

Scott, A. C. (2010). Charcoal recognition, taphonomy and uses in palaeoenvironmental analysis. *Palaeogeography, Palaeoclimatology, Palaeoecology*, 291(1-2), 11–39. https://doi.org/10.1016/j.palaeo.2009.12.012

Scott, A. C., & Glasspool, I. J. (2007). Observations and experiments on the origin and formation of inertinite group macerals. International Journal of Coal Geology, 70(1-3), 53-66. https://doi.org/10.1016/j.coal.2006.02.009

Scott A. C., & Jones T. P. (1994). The nature and influence of fire in Carboniferous ecosystems. *Palaeogeography, Palaeoclimatology, Palaeoecology*, 106(1-4), 91-112. https://doi.org/10.1016/0031-0182(94)90005-1

Shen, W., Sun, Y., Lin, Y., Liu, D., & Chai, P. (2011). Evidence for wildfire in the Meishan section and implications for Permian-Triassic events. *Geochimica et Cosmochimica Acta*, 75(7), 1992-2006. https://doi.org/10.1016/j.gca.2011.01.027

Sheng, C. (2007). Char structure characterised by Raman spectroscopy and its correlations with combustion reactivity. *Fuel*, 86(15), 2316-2324. https://doi.org/10.1016/j.fuel.2007.01.029

de Sousa, D.V., Guimarães, L. M., Félix, J. F., Ker, J. C., Schaefer, C. E. R. G., & Rodet, M. J. (2020). Dynamic of the structural alteration of biochar in ancient Anthrosol over a long timescale by Raman spectroscopy. *PLoS One*, 15(3), e0229447. https://doi.org/10.1371/journal.pone.0229447

Taylor, S. W., Wotton, B. M., Alexander, M. E., & Dalrymple, G. N. (2004). Variation in wind and crown fire behaviour in a northern jack pine-black spruce forest. *Canadian Journal of Forest Research*, 34(8), 1561-1576. https://doi.org/10.1139/x04-116

Tran, H. C., & White, R. H. (1992). Burning rate of solid wood measured in a heat release rate calorimeter. *Fire and Materials*, 16(4), 197–206. https://doi.org/10.1002/fam.810160406

Tuinstra, F., & Koenig, J. L. (1970). Raman spectrum of graphite. *The Journal of Chemical Physics*, 53(3), 1126-1130. https://doi.org/10.1063/1.1674108

Uhl, D., Hartkopf-Fröder, C., Littke, R., & Kustatscher, E. (2014). Wildfires in the late Palaeozoic and Mesozoic of the Southern Alps—the Anisian and Ladinian (Mid Triassic) of the Dolomites (Northern Italy). *Palaeobiodiversity and Palaeoenvironments*, 94, 271-278. https://doi.org/10.1007/s12549-014-0155-y

Wilkins, R.W.T., Boudou, R., Sherwood, N., & Xiao, X. (2014) Thermal maturity evaluation from inertinites by Raman spectroscopy: the 'RaMM' technique. *International Journal of Coal Geology*, 128-129, 143-152. https://doi.org/10.1016/j.coal.2014.03.006

Wilkins, R.W.T., Sherwood, N., & Li, Z. (2018) RaMM (Raman maturity method) study of samples used in an interlaboratory exercise on a standard test method for determination of vitrinite reflectance on dispersed organic matter in rocks. *Marine and Petroleum Geology*, 91, 236-250. https://doi.org/10.1016/j.marpetgeo.2017.12.030

Wilkins, R.W.T., Wang, M., Gan, H., & Li, Z. (2015) A RaMM study of thermal maturity of dispersed organic matter in marine source rocks. *International Journal of Coal Geology*, 150–151, 252-264. https://doi.org/10.1016/j.coal.2015.09.007

Wopenka, B., & Pasteris, J. D. (1993). Structural characterization of kerogens to granulite-facies graphite: Applicability of Raman microprobe spectroscopy. *American Mineralogist*, 78(5-6), 533–557.

966 Wotton, B., Gould, J. S., McCaw, W. L., Cheney, N. P., & Taylor, S. W. (2012). Flame
967 temperature and residence time of fires in dry eucalypt forest. *International Journal of*
968 *Wildland Fire*, 21(3), 270-281. https://doi.org/10.1071/WF10127

969 Yamauchi, S., Kikuchi, Y., & Kurimoto, Y. (2000). Raman spectral changes of Sugi bark
970 during thermal degradation and carbonization. *Journal of the Society of Materials*
971 *Science, Japan*, 49(9. Appendix), 227-228.
972 https://doi.org/10.2472/jsms.49.9Appendix_227

973 Yamauchi, S., & Kurimoto, Y. (2003). Raman spectroscopic study on pyrolyzed wood and
974 bark of Japanese cedar: temperature dependence of Raman parameters. *Journal of*
975 *Wood Science*, 49, 235-240. https://doi.org/10.1007/s10086-002-0462-1

976 Zaida, A., Bar-Ziv, E., Radovic, L. R., & Lee, Y-J. (2007). Further development of Raman
977 microprobe spectroscopy for characterization of char reactivity. *Proceedings of the*
978 *Combustion Institute*, 31(2), 1881-1887. https://doi.org/10.1016/j.proci.2006.07.011

979 Zhang, Y., & Li, Z. (2019). Raman spectroscopic study of chemical structure and thermal
980 maturity of vitrinite from a suite of Australia coals. *Fuel*, 241, 188-198.
981 https://doi.org/10.1016/j.fuel.2018.12.037